arXiv:1605.01237v2 [cond-mat.quant-gas] 6 Jan 2017

Quantum domain walls induce incommensurate supersolid phase on the anisotropic triangular lattice

Xue-Feng Zhang (张学锋),[1,2,3,*] Shijie Hu (胡时杰),[1,†] Axel Pelster,[1] and Sebastian Eggert[1]

[1] *Physics Dept. and Res. Center OPTIMAS, Univ. of Kaiserslautern, 67663 Kaiserslautern, Germany*
[2] *Max-Planck-Institute for the Physics of Complex Systems, 01187 Dresden*
[3] *State Key Laboratory of Theoretical Physics, Institute of Theoretical Physics, Chinese Academy of Sciences, Beijing 100190, China*

(Dated: January 9, 2017)

We investigate the extended hard-core Bose-Hubbard model on the triangular lattice as a function of spatial anisotropy with respect to both hopping and nearest-neighbor interaction strength. At half-filling the system can be tuned from decoupled one-dimensional chains to a two-dimensional solid phase with alternating density order by adjusting the anisotropic coupling. At intermediate anisotropy, however, frustration effects dominate and an incommensurate supersolid phase emerges, which is characterized by incommensurate density order as well as an anisotropic superfluid density. We demonstrate that this intermediate phase results from the proliferation of topological defects in the form of quantum bosonic domain walls. Accordingly, the structure factor has peaks at wave vectors, which are linearly related to the number of domain walls in a finite system in agreement with extensive quantum Monte Carlo simulations. We discuss possible connections with the supersolid behavior in the high-temperature superconducting striped phase.

PACS numbers: 67.80.kb,67.85.-d, 05.30.Jp, 75.40.Mg

Ever since the observation of the superfluid-Mott transition in an optical atomic lattice [1], ultra-cold gases have been considered as promising candidates for the controlled quantum simulation of condensed matter systems with interesting many-body physics [2]. Even though theorists are quite creative in inventing new models, experimental progress is surprisingly quick to follow. Recently, frustrated lattices [3] have been of broad interest due to the emergence of new exotic phases, such as spin-liquids [4–9], topological excitations [10, 11], and supersolids [12–23]. Frustrated lattices with spatial anisotropy are in the center of attention [24–44] since a frustrating interchain coupling allows to study effects of both a changing dimensionality and a tunable frustration.

A straightforward frustrated geometry is provided by the triangular lattice, which is realized by various types of materials, ranging from antiferromagnets such as $Ba_3CoSb_2O_9$ [45–47] and $Cs_2CuCl_{4-x}Br_x$ [28–30] to organic salts [31–37]. For antiferromagnetic xy-coupling with spatial anisotropy there has been a controversial discussion on a possible spin liquid phase [28–40] or an incommensurate phase [42, 43]. For hard-core bosons in optical lattices the hopping parameter plays the role of a ferromagnetic xy-coupling. In this case, nearest neighbor interacting bosons are realizable, for instance, with magnetic erbium atoms [48]. On the triangular lattice [49, 50] they have been predicted to show supersolid behavior [12–21], which is characterized by two independent spontaneously broken symmetries – U(1) and translation – with corresponding superfluid and density order. For an anisotropic triangular lattice the commensurate supersolid phase is found to be unstable [26, 27], and the solid order turns out to be incommensurate [41].

Supersolid phases with two independently broken order parameters were first discussed for solid He [51, 52] and were more recently shown to exist theoretically [12–21] and experimentally [53, 54] in optical lattices for ultra-cold gases. Although high-temperature superconductors [55–57] are not often mentioned in this context, the coexistence of superconductivity and anti-ferromagnetic density order, so-called superstripes, are the defining characteristics of an *incommensurate* supersolid. Remarkably, the analogous physical phenomenon of incommensurate density order together with a finite superfluid density can be observed in a simple hard-core boson model. In the following we present a quantitative analytical model for this behavior in terms of topological defects in their simplest form, namely an increasing number of domain walls. Obviously the microscopic model of high-temperature superconductors is quite different, but the detailed understanding of the underlying mechanism via a spontaneous appearance of domain walls [55–57] is a helpful unifying feature of these many-body phenomena.

In this paper we analyze the quantum phase diagram of hard-core bosons with anisotropic hopping $t, t' \geq 0$ and nearest neighbor interactions $V, V' \geq 0$ on a triangular lattice

$$\begin{aligned}\hat{H} &= \sum_{\langle i,j\rangle_x} [-t(\hat{b}_i^\dagger \hat{b}_j + \text{h.c.}) + V(\hat{n}_i - 1/2)(\hat{n}_j - 1/2)] \\ &+ \sum_{\langle i,j\rangle_\wedge} [-t'(\hat{b}_i^\dagger \hat{b}_j + \text{h.c.}) + V'(\hat{n}_i - 1/2)(\hat{n}_j - 1/2)], \quad (1)\end{aligned}$$

where $\langle i,j\rangle_x$ and $\langle i,j\rangle_\wedge$ represent the nearest neighbor sites on the horizontal bonds and the diagonal inter-chain bonds, respectively, as shown in the inset of Fig. 1 (a). According to Eq. (1) we consider this model without ad-

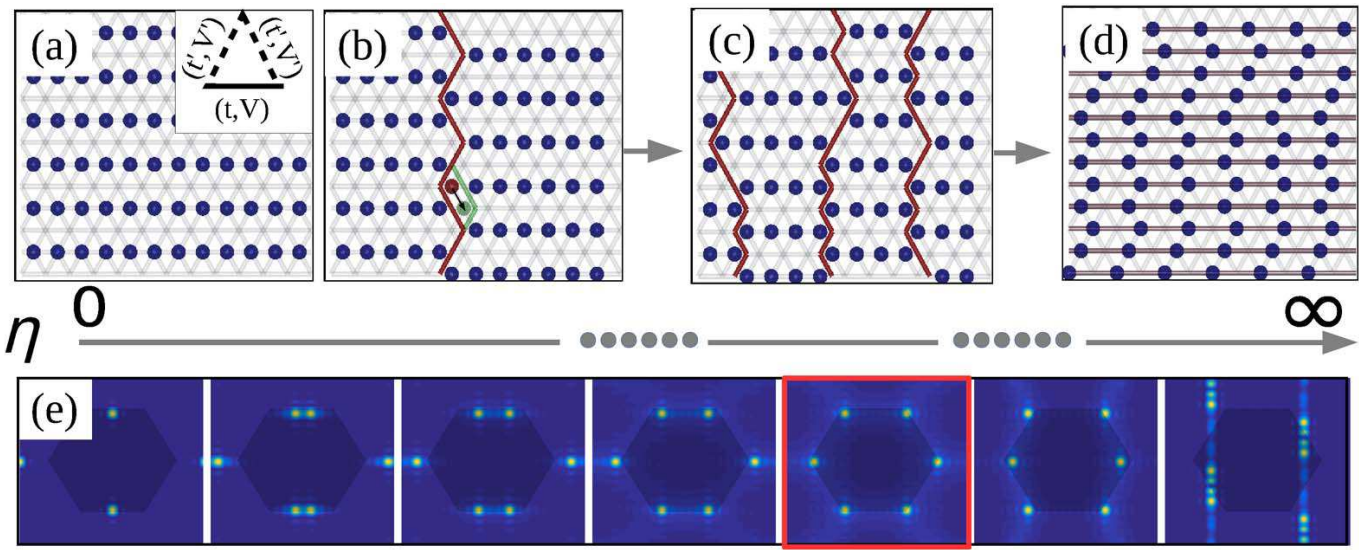

FIG. 1: (a) Configuration of checkered solid phase when $V' \gg V$ (inset: notation for hoppings and interactions); (b) Single bosonic domain wall (red line) is excited for larger η. Kinks can fluctuate by particle hopping to new shape (green); (c) Multi-domain wall case; (d) Decoupled chain phase when $V' \ll V$, thick lines indicate strong interactions and order in x-direction; (e) Structure factors of phases with different numbers of domain walls (from left to right: $N_D = 0$, 2, 4, 6, 8, 10, and 12) for lattice size $L_x = L_y = 12$ and pbc. First Brillouin zone is indicated by shading and red box marks commensurate supersolid ($\eta = 1$).

ditional chemical potential, which corresponds to half-filling, where the most interesting physics is expected to occur due to particle-hole symmetry. The anisotropy parameter is denoted by $\eta \equiv t/t' = V/V'$ and the number of lattice sites in x- and y-directions are assumed to be equal $L = L_x = L_y$, yielding $N = L^2$.

In the strong-coupling limit $t = t' = 0$, the hard-core boson model is equivalent to the Ising model on the triangular lattice. For the isotropic case $\eta = 1$ any state, which fulfills the constraint of one or two bosons per triangle, minimizes the energy. This leads to a finite zero-temperature entropy of $S/N = 0.323\ k_{\rm B}$ [58], whose degeneracy is removed for any $\eta \neq 1$. When $\eta < 1$, the bosons form a checkered order, which alternates in the inter-chain direction as is shown in Fig. 1(a). This leads to distinct peaks of the structure factor $S(\mathbf{Q}) = \langle |\sum_{k=1}^{N} n_k e^{i\mathbf{Q}\cdot\mathbf{r}_k}|^2\rangle/N$ at the wave vectors $(\pm 2\pi, 0)$ and $(0, \pm 2\pi/\sqrt{3})$, related by a reciprocal lattice vector, as is shown in the left panel of Fig. 1(e). When $\eta > 1$, the particles form a quasi-density wave alternating in x-direction with order at $\mathbf{Q} = (\pm\pi, q_y)$ on each horizontal chain of the lattice according to Fig. 1(d) and the right panel of Fig. 1(e). Here q_y is arbitrary, i.e. there is no order in the y-direction, since the energy does not change when all particles in one chain move together. In this case the ground-state entropy is proportional to the number of chains L_y.

Finite hopping $t > 0$ also removes the degeneracy, which leads to a finite range of $\eta \neq 1$, where the ground state is dominated by quantum fluctuations. For $\eta = 1$ it is well known that the system supports a commensurate supersolid phase [12–21] at ordering wave vector $\mathbf{Q} = (\pm 4\pi/3, 0)$, which is also stable in a range of non-zero chemical potential, i.e. away from half-filling. Remarkably, the supersolid can become incommensurate for $\eta \neq 1$ [41], which will be described analytically in this work.

To this end we propose that an incommensurate supersolid can be modeled by topological excitations of the checkered ordered phase. In particular, the potential energy cost of inserting a domain wall in form of a phase shift as shown in Fig. 1(b) is given by $(V' - V)L_y/2 = V'(1-\eta)L_y/2$, i.e. it is proportional to the number of changed bonds in y-direction. At the same time there is a gain in kinetic energy since each kink can fluctuate via particle hopping at the domain wall as indicated by red and green sites in Fig. 1(b). In fact the left/right direction of the domain can be mapped to spin states (up/down) and analyzing all possible cases of hopping it turns out that the kinetic energy is described exactly by two independent xy-chains for each domain wall. The xy-chain in turn is exactly solvable, including correlation functions, and the energy is known to be $-2L_y t'/\pi$ [10]. The effective energy for a finite density $\rho_D = N_D/L_x$ of domain walls is therefore given by

$$E(\rho_D) = L_x L_y V' \rho_D \left[\frac{1-\eta}{2} - \frac{2t'}{\pi V'} + f(\rho_D)\right]. \qquad (2)$$

Here the last term accounts for an effective repulsive interaction energy between two neighboring domain walls separated by a distance $1/\rho_D$. The yet unknown function

$f(\rho_D)$ must obey $f(\rho_D=0)=0$ and will be determined numerically below. Using the condition $\partial_{\rho_D} E = 0$ in order to extremize the domain wall energy (2) yields a relation between η and ρ_D

$$\eta = 1 - \frac{4t'}{V'\pi} + 2\frac{\partial}{\partial\rho_D}\Big[\rho_D f(\rho_D)\Big]. \qquad (3)$$

The first domain wall appears when it becomes energetically favorable to spontaneously allow fluctuations. This onset of the phase transition can be determined from Eq. (3) with $\rho_D = 0$ and $f = 0$ resulting in a critical value $\eta_{c1} = 1 - 4t'/V'\pi$, which agrees well with numerical simulations, see below. Note that additional domain walls at equal distance will not immediately destroy the order completely. Instead, each domain wall effectively removes half of a spatial density oscillation in a finite system without changing its wave length, so that the positions of the structure factor peaks are shifted by $\pm\pi/L_x$ for each domain wall in the system. This is the microscopic origin of the observed incommensurable order, with predicted wave vectors $\mathbf{Q} = \pi(\pm 2 - \rho_D, 0)$ and $\pi(\pm\rho_D, \pm 2/\sqrt{3})$ changing with ρ_D. At the same time transport of bosons becomes possible along the domain walls in y-direction, leading to a corresponding anisotropic superfluid density which will be analyzed in more detail below.

For the numerical results we implemented a Quantum Monte Carlo (QMC) code using the Stochastic Cluster Series Expansion algorithm [59–61], which is further discussed in the Appendix [62]. Since the bosonic hopping is positive, there is no kinetic frustration and the model does not suffer from the minus sign problem. We use 5×10^5 thermalization steps and 10^6 measuring steps on lattices up to length $L = 24$ with periodic boundary conditions (pbc) in both directions. Since topological quantum numbers, such as domain walls, are difficult to change with ordinary QMC updates, we developed an extension of the parallel tempering method [62, 63]. All numerical data in Figs. 2 and 3 are plotted with error bars which are too small to be distinguishable. The inverse temperature β is measured in units of the larger repulsive energy $V_{\max} = \max(V, V')$. The transition from the supersolid phase to a uniform superfluid phase occurs at $t'/V' \approx 0.11$ [12]. In our simulations we therefore focus on the choice of $t/V = t'/V' = 0.08$, which is in the center of the supersolid phase we are interested in. Results for other values of t'/V' are discussed in the Appendix [62].

In order to determine the domain wall density we define the operator

$$\rho_D = \sum_{i_y=1}^{L_y}\sum_{i_x=1}^{L_x} \frac{n_{(i_x,i_y)}\bar{n}_{(i_x+1,i_y)} + n_{(i_x+1,i_y)}\bar{n}_{(i_x,i_y)}}{L_x L_y}, \quad (4)$$

where $\bar{n} = 1-n$. For hard core bosons $n_{(i_x,i_y)}\bar{n}_{(i_x+1,i_y)} + n_{(i_x+1,i_y)}\bar{n}_{(i_x,i_y)}$ corresponds to $1 - \delta_{n_{(i_x,i_y)},\bar{n}_{(i_x+1,i_y)}}$, so

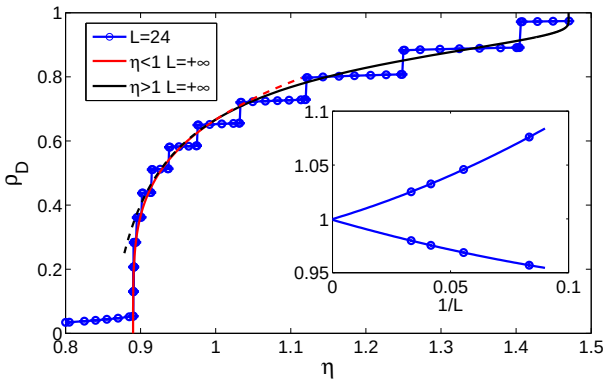

FIG. 2: Bosonic domain wall density (4) as function of anisotropy parameter η for $L = 24$ with pbc at $t'/V' = 0.08$ and $\beta V_{\max} = 400$ from QMC (dots) compared to the analytical predictions from Eqs. (5) (red) and (6) (black), respectively. Inset: Finite-size scaling of left and right points of the commensurate supersolid plateau ($\rho_D = 2/3$) with a second order polynomial fit.

ρ_D effectively counts the number of density changes along the x-direction. Note that domain walls have to be created in pairs because of pbc, so that $N_D = \rho_D L_x$ should be an even integer. The QMC results in Fig. 2 clearly show plateaus of quantized domain wall numbers with discrete jumps as a function of η. This is remarkable since the densities fluctuate strongly in the QMC simulations, but the correlation function in Eq. (4) yields robust discrete quantum numbers. The expected integer values are only slightly renormalized by quantum fluctuations, which are further suppressed for smaller t'/V' [62]. The phase transition occurs at $\eta_{c1} \approx 0.89$ for $t'/V' = 0.08$ in good agreement with the analysis above. The plateaus and the jumps between them become more and more continuous for increasing lengths. A finite-size scaling of the left and right ends of the commensurate plateau at $\rho_D = 2/3$ is shown in the inset of Fig. 2, which clearly demonstrates that a continuous function $\rho_D(\eta)$ is approached in the thermodynamic limit. Also the jump to the first plateau and the change in the superfluid order parameter vanishes in the thermodynamic limit at the critical point η_{c1} [62], which is the hallmark of a second-order phase transition. The interaction energy $f(\rho_D)$ can be analyzed from QMC results with the help of Eq. (2), which yields a near perfect agreement with a powerlaw behavior $f(\rho_D) \propto \rho_D^4$ [62], i.e. a $1/\text{distance}^4$-law. The proportionality constant is fixed by imposing the communicability condition $\rho_D(\eta=1) = 2/3$, which together with Eq. (3) yields a prediction for the behavior in the thermodynamic limit

$$\rho_D(\eta) = \frac{2}{3}\left(\frac{\eta-\eta_{c1}}{1-\eta_{c1}}\right)^{1/4}. \qquad (5)$$

This analytic results is shown as a red line in Fig. 2 with

very good agreement in the region of dilute domain walls, i.e. $\rho_D < 2/3$ and $\eta_{c1} < \eta < 1$.

At full saturation $\rho_D = 1$ a second transition to the decoupled chain phase occurs at η_{c2}. This phase has an independent alternating density order in the ground state. The basic excitation is again a domain wall, but this time for each chain separately in the form of equal neighboring densities $n_{i,j} = n_{i,j+1}$, i.e. a phase shift in the alternating order along x-direction. Such a neighboring density pair can be transported ballistically along the entire chain, which yields a large superfluid density along the x-direction and again a shift in the ordering wave vector. A single pair has a potential energy cost of $(V - V')/2$ and yields a kinetic energy gain in the $q_x = 0$ state of $-2t$, resulting in a critical density of $\eta_{c2} = 1/(1 - 4t'/V')$. This yields for $t'/V' = 0.08$ the value $\eta_{c2} \approx 1.47$ in excellent agreement with our numerical results. We can also define the interaction energy between two neighboring density pairs $g(\rho_D)$, and determine it along similar lines as above. A fit to numerical results yields for $g(\rho_D)$ an exponential decay [62] which gives a domain wall function

$$\rho_D(\eta) = 1 + \frac{1}{3}\left[1 + W_{-1}\left(-\frac{2(\eta_{c2} - \eta)}{e^2(\eta_{c2} - 1)}\right)\right]^{-1} \qquad (6)$$

in the limit of few density pairs, i.e. relatively close to saturation $2/3 \lesssim \rho_D < 1$. Here W_{-1} represents the branch -1 of the Lambert W function and is plotted in Fig. 2 as a black line for $t'/V' = 0.08$ and $1 \leq \eta < \eta_{c2}$.

Further evidence for the existence of domain walls comes from the corresponding structure factor $S(\mathbf{Q})/N$, which is shown in Fig. 1(e) at one parameter point for each domain wall number. In the incommensurate supersolid the peak positions shift with anisotropy, which reflects the change from checkered order to independent chains. As predicted by the domain wall theory, the peak positions are directly related to the respective number of domain walls [62]. All these observations strongly support the quantum nature of domain walls, and rule out classical explanations of incommensurate order, such as a continuous spiral rotation of the spin [64].

In the supersolid phase both the translational symmetry and the U(1) gauge symmetry are broken. Therefore it is also interesting to analyze the corresponding U(1) order parameter, namely the total superfluid density $\rho_s = \rho_s^x + \rho_s^y$ and its components $\rho_s^{x(y)} = W_{x(y)}^2/(4\beta t)$, where $W_{x(y)}$ stands for the winding number in $x(y)$-direction [65]. According to Fig. 3, the total superfluid density ρ_s behaves opposite to the structure factor, which indicates that the two order parameters are competing [17]. The total superfluid density is reduced in both anisotropic limits and increases for a decreasing anisotropy. In general the superfluid density is an anisotropic tensor [66, 67], which in fact reflects the properties of the domain walls presented above: For $\eta < 1$ the

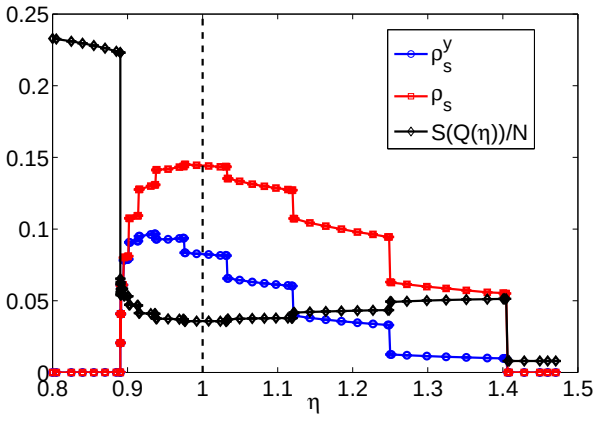

FIG. 3: Total superfluid density $\rho_s = \rho_s^x + \rho_s^y$, its value in y-direction ρ_s^y, and structure factor $S(\mathbf{Q})/N$ at $t/V = 0.08$, $\beta V_{\max} = 400$, and $L = 24$.

superfluidity along the y-direction dominates, which is caused by hopping of domain wall kinks, increasing with the number of domain walls. The maximum of the total superfluid density occurs at $\eta = 1$, where fluctuations in both directions are equally possible. For $\eta > 1$ the superfluidity is caused by neighboring density pairs, predominantly in the x-direction. Interestingly, we observe strong jumps in ρ_s^y at $\eta = 1.25$ and $\eta = 1.1$ corresponding to the occurance of the second and third density pair in a finite system. This can only be explained by correlations of the density pairs perpendicular to the chains, which signals the buildup of domain walls discussed above for $\eta < 1$. The jumps are a finite-size effect, however, so the behavior becomes continuous in the thermodynamic limit.

In the context of superfluidity it is interesting to remember that also in the striped phase of high-temperature superconductors domain walls and superconductivity coexist [55–57]. We have seen that in our bosonic model both domain walls and neighboring density pairs naturally emerge and cause superfluidity where the fluctuations are largest. Even though the microscopic pairing mechanism is more involved for superconductors, our results suggest that it is related to the coherent motion of neighboring domain walls and an effective reduction to one dimension.

In summary, we analyzed the quantum phase diagram of the extended anisotropic Bose-Hubbard model on the triangular lattice. Due to frustration a non-trivial incommensurate supersolid phase appears, which can be well described analytically by topological defects in the form of domain walls. For small η the domain walls along the y-direction are described by the exactly solvable xy-chain model together with a $1/\text{distance}^4$-interaction between them. For large η an independent description in terms of neighboring density pairs with an exponential inter-

action is possible. The numerical results for the phase transition lines, the domain wall density, the incommensurate ordering wave vectors, and the superfluid density agree with this theory. In the low density region it will, in principle, be possible to use a more detailed analysis of the xy-model, if higher-order correlation functions, finite temperature behavior, or dynamical properties need to be calculated. For larger domain wall densities a coherent pairing mechanism causes a dominant superfluid density in the x-direction, which is due to the movement of neighboring density pairs. This mechanism may be related to pairing in the striped phases in high temperature superconductors, where superconductivity coexists with incommensurate order and domain walls.

We are thankful for useful discussions with Chisa Hotta, Ying Jiang, Frank Pollmann, and Yue Yu. This work was supported by the Chinese Academy of Sciences via the Open Project Program of the State Key Laboratory of Theoretical Physics, by the Nachwuchsring of the TU Kaiserslautern, and by the German Research Foundation (DFG) via the Collaborative Research Centers SFB/TR49, SFB/TR173, and SFB/TR185. The authors gratefully acknowledge the computing time granted by the John von Neumann Institute for Computing (NIC) on the supercomputer JURECA at Jülich Supercomputing Centre (JSC) and by the Allianz für Hochleistungsrechnen Rheinland-Pfalz (AHRP),

* Corresponding author: xuefeng@pks.mpg.de
† Corresponding author: shijiehu@physik.uni-kl.de

[1] M. Greiner, O. Mandel, T. Esslinger, T. W. Hänsch, and I. Bloch, Nature **415**, 39 (2002).
[2] I. Bloch, J. Dalibard, and S. Nascimbène, Nature Phys. **8**, 267 (2012).
[3] R. Moessner and A. P. Ramirez, Phys. Today **59**, 24 (2006).
[4] L. Balents, Nature (London) **464**, 199 (2010).
[5] G. Evenbly and G. Vidal, Phys. Rev. Lett. **104**, 187203 (2010).
[6] S. Yan, D. A. Huse, and S. R. White, Science **332**, 1173 (2011).
[7] Y. Iqbal, F. Becca, S. Sorella, and D. Poilblanc, Phys. Rev. B **87**, 060405(R) (2013).
[8] S. Capponi, V. R. Chandra, A. Auerbach, and M. Weinstein, Phys. Rev. B **87**, 161118(R) (2013).
[9] Y.-C. He and Y. Chen, Phys. Rev. Lett. **114**, 037201 (2015).
[10] X.-F. Zhang and S. Eggert, Phys. Rev. Lett. **111**, 147201 (2013).
[11] C. Nisoli, R. Moessner, and P. Schiffer, Rev. Mod. Phys. **85**, 1473 (2013).
[12] S. Wessel and M. Troyer, Phys. Rev. Lett. **95**, 127205 (2005).
[13] D. Heidarian and K. Damle, Phys. Rev. Lett. **95**, 127206 (2005).
[14] R. G. Melko, A. Paramekanti, A. A. Burkov, A. Vishwanath, D. N. Sheng, and L. Balents, Phys. Rev. Lett. **95**, 127207 (2005).
[15] M. Boninsegni and N. Prokof'ev, Phys. Rev. Lett. **95**, 237204 (2005).
[16] A. Sen, P. Dutt, K. Damle, and R. Moessner, Phys. Rev. Lett. **100**, 147204 (2008).
[17] X.-F. Zhang, Y. C. Wen, and S. Eggert, Phys. Rev. B **82**, 220501(R) (2010).
[18] L. Bonnes and S. Wessel, Phys. Rev. B **84**, 054510 (2011).
[19] X.-F. Zhang, R. Dillenschneider, Y. Yu, and S. Eggert, Phys. Rev. B **84**, 174515 (2011).
[20] D. Yamamoto, I. Danshita, and C.A.R. Sá de Melo, Phys. Rev. A **85**, 021601(R) (2012).
[21] D. Yamamoto, T. Ozaki, C.A.R. Sá de Melo, and I. Danshita, Phys. Rev. A **88**, 033624 (2013).
[22] L.F. Tocchio, C. Gros, X.-F. Zhang, and S. Eggert, Phys. Rev. Lett. **113**, 246405 (2014).
[23] D. Sellmann, X-F. Zhang, and S. Eggert, Phys. Rev. B **91**, 081104(R) (2015).
[24] O.A. Starykh and L. Balents, Phys. Rev. Lett. **93**, 127202 (2004).
[25] C. Hotta and F. Pollmann, Phys. Rev. Lett. **100**, 186404 (2008).
[26] J. Y. Gan, Phys. Rev. B **78**, 014513 (2008).
[27] J. Y. Gan and J. F. Gan, J. Phys. Soc. Jpn. **78**, 094602 (2009).
[28] R. Coldea, D. A. Tennant, A. M. Tsvelik, and Z. Tylczynski, Phys. Rev. Lett. **86**, 1335 (2001).
[29] N. A. Fortune, S. T. Hannahs, Y. Yoshida, T. E. Sherline, T. Ono, H. Tanaka, and Y. Takano, Phys. Rev. Lett. **102**, 257201 (2009).
[30] P.T. Cong *et al.*, Phys. Rev. B **83**, 064425 (2011).
[31] Y. Shimizu, K. Miyagawa, K. Kanoda, M. Maesato, and G. Saito, Phys. Rev. Lett. **91**, 107001 (2003).
[32] T. Yoshioka, A. Koga, and N. Kawakami, Phys. Rev. Lett. **103**, 036401 (2009).
[33] E. P. Scriven and B. J. Powell, Phys. Rev. Lett. **109**, 097206 (2012).
[34] T. Isono, H. Kamo, A. Ueda, K. Takahashi, M. Kimata, H. Tajima, S. Tsuchiya, T. Terashima, S. Uji, and H. Mori, Phys. Rev. Lett. **112**, 177201 (2014).
[35] Y. Yoshida, H. Ito, M. Maesato, Y. Shimizu, H. Hayama, T. Hiramatsu, Y. Nakamura, H. Kishida, T. Koretsune, C. Hotta, and G. Saito, Nat. Phys. **11**, 679 (2015).
[36] H.O. Jeschke, M. de Souza, R. Valentí, R.S. Manna, M. Lang, J.A. Schlueter, Phys. Rev. B **85**, 035125 (2012).
[37] A. C. Jacko, L. F. Tocchio, H. O. Jeschke, R. Valentí, Phys. Rev. B **88**, 155139 (2013).
[38] L. F. Tocchio, H. Feldner, F. Becca, R. Valentí, and C. Gros, Phys. Rev. B **87**, 035143 (2013).
[39] L. F Tocchio, C. Gros, R. Valentí, and F. Becca, Phys. Rev. B **89**, 235107 (2014).
[40] E. Ghorbani, L.F. Tocchio, and F. Becca, Phys. Rev. B **93**, 085111 (2016).
[41] S. V. Isakov, H.-C. Chien, J.-J. Wu, Y.-C. Chen, C.-H. Chung, K. Sengupta, and Y. B. Kim, Europhys. Lett. **87**, 36002 (2009).
[42] A. Weichselbaum and S. R. White, Phys. Rev. B **84**, 245130 (2011).
[43] K. Harada, Phys. Rev. B **86**, 184421 (2012).
[44] A. Metavitsiadis, D. Sellmann, and S. Eggert, Phys. Rev. B **89**, 241104(R) (2014).
[45] Y. Shirata, H. Tanaka, A. Matsuo, and K. Kindo Phys. Rev. Lett. **108**, 057205 (2012).
[46] H. D. Zhou, C. Xu, A. M. Hallas, H. J. Silverstein, C. R.

Wiebe, I. Umegaki, J. Q. Yan, T. P. Murphy, J.-H. Park, Y. Qiu, J. R. D. Copley, J. S. Gardner, and Y. Takano, Phys. Rev. Lett. **109**, 267206 (2012).
[47] T. Susuki, N. Kurita, T. Tanaka, H. Nojiri, A. Matsuo, K. Kindo, and H. Tanaka, Phys. Rev. Lett. **110**, 267201 (2013).
[48] S. Baier, M. J. Mark, D. Petter, K. Aikawa, L. Chomaz, Zi Cai, M. Baranov, P. Zoller, and F. Ferlaino, Science **352**, 201 (2016).
[49] C. Becker, P. Soltan-Panahi, J. Kronjäger, S. Dörscher, K. Bongs, and K. Sengstock, New J. Phys. **12**, 065025 (2010).
[50] A. Eckardt, P. Hauke, P. Soltan-Panahi, C. Becker, K. Sengstock, and M. Lewenstein, Europhys. Lett. **89**, 10010 (2010).
[51] A. F. Andreev and I. M. Lifshitz, Sov. Phys. JETP **29**, 1107 (1969).
[52] G. V. Chester, Phys. Rev. A **2**, 256 (1970).
[53] J. Klinder, H. Keßler, M. R. Bakhtiari, M. Thorwart, and A. Hemmerich, Phys. Rev. Lett. **115**, 230403 (2015).
[54] R. Landig, L. Hruby, N. Dogra, M. Landini, R. Mottl, T. Donner, and T. Esslinger, Nature **532**, 476 (2016).
[55] S. R. White and D. J. Scalapino, Phys. Rev. Lett. **81**, 3227 (1998).
[56] For a review see M. Vojta, Adv. Phys. **58**, 699 (2009).
[57] H. Yamase, A. Eberlein, and W. Metzner, Phys. Rev. Lett. **116**, 096402 (2016).
[58] R. Moessner and S. L. Sondhi, Phys. Rev. B **63**, 224401 (2001).
[59] A. W. Sandvik, Phys. Rev. B **59**, R14157 (1999).
[60] O. F. Syljuåsen and A. W. Sandvik, Phys. Rev. E **66**, 046701 (2002).
[61] K. Louis and C. Gros, Phys. Rev. B **70**, 100410(R) (2004).
[62] See Appendix for a discussion of further details about the performed Quantum Monte Carlo simulations, the behavior as a function of length and t/V, and the analysis for determining the effective interaction energy between the domain walls.
[63] P. Sengupta, A.W. Sandvik, and D.K. Campbell Phys. Rev. B **65**, 155113 (2002).
[64] W. Zheng, R. H. McKenzie, and R. R. P. Singh, Phys. Rev. B **59**, 14367 (1999).
[65] E. L. Pollock and D. M. Ceperley, Phys. Rev. B **36**, 8343 (1987).
[66] M. Ueda, *Fundamentals and New Frontiers of Bose-Einstein Condensation* (World Scientific, Singapore, 2010).
[67] X.-F. Zhang, T. Wang, S. Eggert, and A. Pelster, Phys. Rev. B **92**, 014512 (2015).

APPENDIX

In the Appendix additional information on the performed Quantum Monte Carlo (QMC) simulations are given. Further results as a function of hopping strength and system size are shown. In addition to periodic boundary conditions, cylindrical boundary conditions also are considered. Finally, details on the derivation of the effective interaction energy between the domain walls are presented.

Quantum Monte Carlo method

For the numerical quantum Monte Carlo (QMC) simulations we implemented the cluster stochastic series expansion method [59–61] by taking into account three sites as the update unit, as it can help increasing the ergodicity [61]. It is well known that QMC may have an infamous minus sign problem if an exchange of two fermions is possible, or if a kinetic frustration occurs, i.e. the overall probability of an off-diagonal exchange along a closed loop is negative. Since we are dealing with bosons with positive hopping our model is without sign problem, despite the triangular geometry.

However, another typical QMC problem of trapping in a local minimum is indeed of concern for our studies. In particular, the domain walls in the incommensurate supersolid phase represent very robust topological defects, so the system may get trapped at a fixed domain wall number, which is difficult to change with a small hopping parameter even using the loop update. In addition, because the wave functions with different domain wall numbers have nearly no overlap, also ordinary parallel tempering [63] does not show much improvement. In order to solve this local minimum problem, a further extension of the parallel tempering method has been developed. To this end we perform the normal QMC simulation in the whole parameter region first and store the configuration at each point. Then, for each parameter point, we use the outcome of neighboring parameter points as the initial configuration and launch additional simulations. When they are finished, we choose the simulation with the lowest average energy as the right one since at low temperatures we are effectively in the ground state limit. We find that without this change of initial configurations the resulting energy curve is discontinuous as a function of parameters, but it becomes continuous after the swap. Only for larger hopping parameters, such as $t/V = 0.1$, the ordinary parallel tempering with loop update can overcome the local minimum.

Phase Transitions

The domain wall picture works well in the strong-coupling limit. In fact up to first-order perturbation theory in the hopping parameter, the ground states with different domain walls have no overlap, so there are no corrections to the quantized values of the domain wall numbers. In the following we illustrate the effect of changing hopping close to (but below) the superfluid transition at $t'/V' \approx 0.11$ [12]. Figure 4 (a) shows that the steps are very clearly visible in the strong-coupling region at $t'/V' = 0.06$, but relaxation of the plateaus is observed when the hopping is increased to $t'/V' = 0.1$. The same is true for the step-like structure for all order parameters in Fig. 4(b-d). For larger hopping $t'/V' = 0.1$ and near

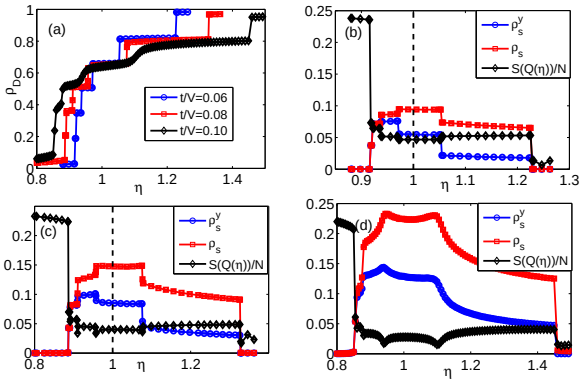

FIG. 4: (a) Bosonic domain wall density as function of anisotropy parameter η at $t/V = 0.06, 0.08, 0.10$. (b-d): Total superfluid density ρ_s, its value in y-direction ρ_s^y, and structure factor $S(\mathbf{Q})/N$ at $t/V = 0.06$ (b), $t/V = 0.08$ (c), $t/V = 0.10$ (d). All QMC results have been obtained for $\beta V_{\max} = 200$ and $L = 12$ with periodic boundary conditions.

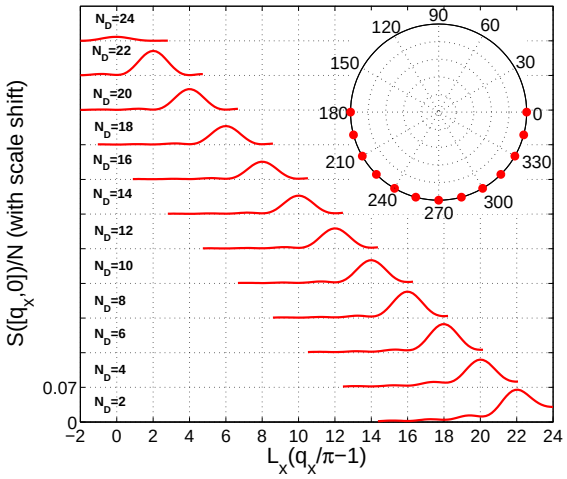

FIG. 5: Structure factor $S(\mathbf{Q})/N$ as function of q_x at $q_y = 0$ for different domain wall densities (shifted relative to each other) at $t/V = 0.08$, $L = 24$, and $\beta V_{\max} = 400$. Inset: Maximum position (red dot) of $S(\mathbf{Q})/N$ in q_x-direction for $q_y = 0$ using values of η corresponding to different domain wall numbers N_D.

the ends of the plateaus, we observe maxima in the superfluid density and minima in the structure factor due to increased fluctuations in Fig. 4(d), but the qualitative signature of domain walls always remains visible.

One of the main results in the paper is that each plateau of the domain wall density is closely related to a corresponding maximum of the structure factor. In order to make this connection clearer, we plot the structure factor $S(\mathbf{Q})/N$ in q_x-direction for $q_y = 0$ using values of η in the center of the corresponding domain wall plateau in Fig. 5. The positions of the peaks match well with the analytic prediction $N_D = L_x(2 - q_x/\pi)$.

Finite-size scaling

In the paper we demonstrated that the quantization of the domain wall density becomes continuous in the thermodynamic limit. This implies that the shift of the structure factor is also continuous at the phase transition, indicating a second-order phase transition. To give additional support we present the finite-size scaling of the superfluid density difference between the two phases at η_{c1} in Fig. 6. Clearly, the second-order polynomial fit shows that the jump also vanishes in the thermodynamic limit for this order parameter, which confirms that the phase transition is of second order.

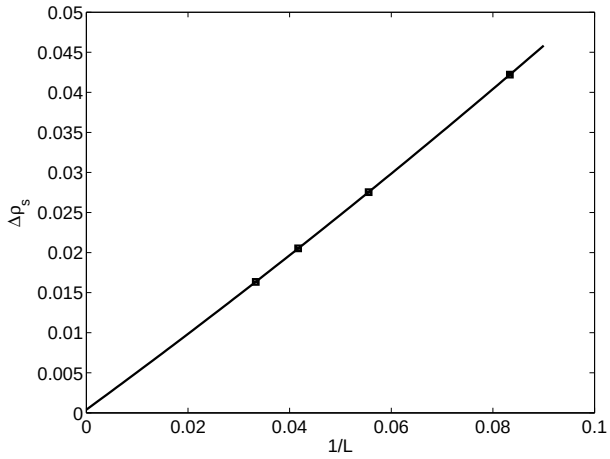

FIG. 6: Finite-size scaling of superfluid density difference between the two phases at η_{c1} for $t/V = 0.08$, $\beta V_{\max} = 200$, and $L/12$.

Cylindrical boundary

Whereas so far we have chosen periodic boundary conditions, we investigate now cylindrical boundary conditions (y-cbc) with open ends in x-direction. In that case single domain walls can be created, so the number of domain walls $N_D = \rho_D L$ can be both even or odd integers, which is indeed seen in the simulations. Furthermore, Fig. 7 shows that the fluctuating domain walls are clearly visible in terms of regions of average half-filling, which separate regions of checkered order, the latter being particularly stable near the edges. All these observations strongly support the quantum nature of domain walls, and rule out classical explanations of incommensurate order, such as a continuous spiral rotation of the spin [64].

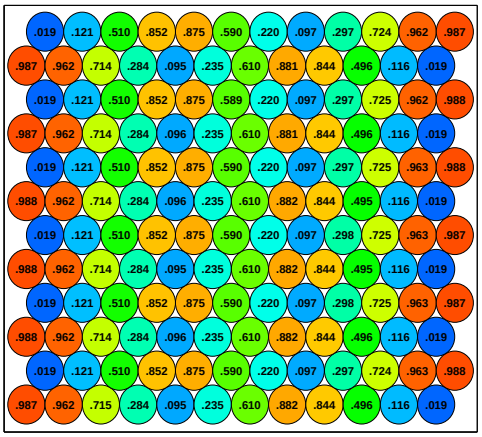

FIG. 7: Average bosonic density distribution at $t/V = 0.08$, $\beta V_{\max} = 200$, $\eta = 0.9$, and $L = 12$ with y-cbc.

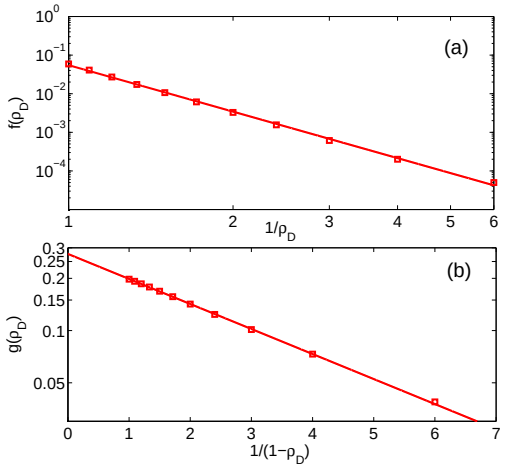

FIG. 8: Fitting of interaction energies between two neighboring (a) domain walls $f(\rho_D)$, (b) density pairs $g(\rho_D)$ for $t/V = 0.08$, $\beta V_{\max} = 400$, and $L = 24$.

Effective interaction energies

In this section, we discuss a phenomenological model how to determine the effective interaction energies between two neighboring domain walls for $\eta < 1$ and density pairs for $\eta > 1$ from QMC data. At first, we discuss the dilute domain wall case $\eta < 1$. The total energy of N_D domain walls is given by

$$E(N_D) = N_D L_y \left[\frac{V' - V}{2} - \frac{2}{\pi} t' + f\left(\frac{N_D}{L_x}\right) V' \right] , \quad (7)$$

as discussed in the Letter. Here the first term corresponds to the potential energy with $V = \eta V'$, the second term denotes the kinetic energy. The third term models the repulsive interaction energy between the domain walls, where the function $f(N_D/L_x)$ takes into account the dependence on the distance L_x/N_D between two domain walls. Thus, we arrive at

$$E(N_D) = V' N_D L_y \left[\frac{1-\eta}{2} - \frac{2}{\pi} t'/V' + f\left(\frac{N_D}{L_x}\right) \right] . \quad (8)$$

Due to periodic boundary conditions the number of domain walls N_D changes by multiples of 2. In order to analyze the respective transitions from $N_D = 2M - 2$ to $N_D = 2M$ with $M = 1, \ldots, M_{\max} = L_x/2$ we have to evaluate the conditions

$$E(N_D = 2M - 2) = E(N_D = 2M) . \quad (9)$$

This yields the position of the jumps between the plateaus

$$\begin{aligned} \eta_M &= 1 - \frac{4}{\pi} t'/V' + 2M f\left(\frac{2M}{L_x}\right) \\ &\quad -(2M-2) f\left(\frac{2M-2}{L_x}\right) . \end{aligned} \quad (10)$$

By formally identifying $\eta_0 = \eta_{c1} = 1 - 4t'/V'\pi$, the respective jump points with different domain wall numbers read explicitly

$$\begin{aligned} \eta_1 &= \eta_{c1} + 2f(2/L_x) \\ \eta_2 &= \eta_{c1} + 4f(4/L_x) - 2f(2/L_x) \\ \eta_3 &= \eta_{c1} + 6f(6/L_x) - 4f(4/L_x) \\ &\vdots \end{aligned} \quad (11)$$

Thus, we deduce from (11) that the effective interaction energy can be reconstructed from the values at which the jumps occur according to

$$f\left(\frac{2M}{L_x}\right) = \sum_{i=1}^{M} \frac{\eta_i}{2M} - \frac{\eta_0}{2} . \quad (12)$$

Using the jump points from QMC simulations (c.f. Fig. 2 in the Letter) we determine via Eq. (12) the effective interaction energy between two domain walls $f(\rho_D)$ for a finite density $\rho_D = N_D/L_x$. The results are shown in Fig. 8 (a) on a double logarithmic scale and clearly indicate a simple power law

$$f(\rho_D) \sim \rho_D^{\alpha} , \quad (13)$$

with $\alpha = 4 \pm 0.1$. The same strategy turns out to be also applicable in the decoupled chain region with neighboring density pair excitations, i.e. $1 < \eta$. The only difference is that now $\eta_0 = \eta_{c2}$ and the effective interaction energy between two neighboring density pairs is denoted by another function $g(\rho_D)$ with $g(\rho_D = 1) = 0$. The corresponding fit in Fig. 8 (b) reveals that the effective interaction energy $g(\rho_D)$ is given by an exponential

$$g(\rho_D) \sim \exp\left(-\frac{1}{\gamma(1-\rho_D)}\right) , \quad (14)$$

with $\gamma = 3 \pm 0.05$. The results in Eqs. (13) and (14) are used in the Letter to derive a relation between η and ρ_D in thermodynamic limit.